Asociación Argentina
de Mecánica Computacional

Mecánica Computacional Vol XXXV, págs. 805-818 (artículo completo)
Martín I. Idiart, Ana E. Scarabino y Mario A. Storti (Eds.)
La Plata, 7-10 Noviembre 2017

COUPLED COMPUTATIONAL FLUID MECHANICS/MULTIBODY DYNAMICS APPROACH FOR NAVAL APPLICATIONS

Alejandro M. Castro[a,b], Ezequiel Martin[a] and Pablo M. Carrica[a]

[a]*IIHR-Hydroscience and Engineering, 100 C. Maxwell Stanley Hydraulics Lab, Iowa City, IA 52242, USA. pablo-carrica@uiowa.edu, www.iihr.uiowa.edu/pcrg*

[b]*Toyota Research Institute, One Kendall Square Building 100, Suite 1-201, Cambridge, MA 02139 USA, http://www.tri.global/*

Keywords: Multibody dynamics, Computational Fluid Dynamics, Cable Modeling, Naval Hydrodynamics.

Abstract. The multibody dynamics (MBD) solver MagnusDyn and the computational fluid dynamics (CFD) code REX, both developed at the University of Iowa, are implicitly coupled. MagnusDyn can solve bodies connected through a variety of joints and cables, while REX is a dynamic overset naval hydrodynamics code with extensive capabilities for motions of surface and underwater vehicles including waves, autopilots and wind. The implementation adds capability to simulate at-sea operations, like takeoff and landing of manned and unmanned aircraft, deployment and recovery of service watercraft, etc. In these maneuvers, interaction between vessels occurs through connecting cables or direct contact. The paper describes the strategy to couple the solvers and presents validation and demonstration cases, including the relaxation of a buoy, and deployment and recovery of an unmanned underwater vehicle.

1 INTRODUCTION

Problems with bodies interacting with a fluid and between them are a challenge for CFD, since body/body interaction imposes demanding conditions on the time step and results in highly coupled systems. Interaction between bodies occurs through contact, connecting cables or fluid forces. Of these, direct contact and cables result in the most challenging conditions.

Since the advent of ships large enough to carry other craft, it has been commonplace for host (or mother) ships to deploy and recover smaller craft. These craft, usually manned surface vessels, are typically launched and recovered via cranes over the side or stern of the host ship. Relatively calm seas have generally been a prerequisite for these operations; in less than ideal conditions, launch and recovery (L&R) is dangerous to both crew and vehicles and can consume a considerable amount of time, waiting until both craft are in a favorable position for the operation to take place. The operation places a strong reliance on highly trained personnel, both on the host ship and the deployed craft for its success.

With the introduction of autonomous or semi-autonomous vehicles in maritime operations, L&R is often desired in sea-conditions that are far from ideal and with demanding time constraints. Obviously, the advantage of having an experienced pilot onboard the deployed craft is lost. Generally, deployed craft are designed to carry out a specific task, not for the L&R operation. Therefore the vehicle is not likely to be ideal from an L&R perspective. All these issues suggest that L&R is no longer an afterthought and must be considered well before any L&R evaluation of a new system is initiated. While physical simulation at model scale is very helpful, conditions under which those simulations can be carried out are limited. As a result, computational simulation is an attractive means of augmenting an understanding of how L&R under a wide range of conditions might proceed, and can help define a safe operational envelope for a given set of craft (host ship and deployed vehicle). Physics-based computational tools, applied in a marine environment, are now able to provide the needed accuracy and fidelity to be useful for engineering work.

Computation of the towing process of marine vehicles has a variety of applications, including towing of service craft, Unmanned Underwater Vehicles (UUVs) and Unmanned Surface Vehicles (USVs), launch and recovery, towing of damaged vessels, etc. Evaluation of a variety of maneuvers involving towed vehicles requires accurate computation of the fluid flow, which is typically carried out with CFD in time steps designed to resolve time scales of interest in the flow. As an example, candidate concepts for ship-board autonomous vehicle operations often involve deployment and recovery over the stern of the host ship. During the cable winch mode the deployed craft is captured by a cable which is released from the host ship and pulled by a winch to the stern of the host ship allowing a mechanism to lift the deployed craft on board the host ship. The flow in this region can be violent and at the length scale of the autonomous service craft, potentially leading to unacceptable motions. Towed and towing vehicles respond to forces and moments originating from/transmitted by the tow cable, resulting in a complex coupling of the rigid body motions of the two craft. The main difficulty arising from coupling a multi-body CFD solver with a cable model is that the time scales involved in the solution of the cable equations are typically one order of magnitude smaller or more than those used in CFD. This smaller time step is unacceptable for CFD since it would make the solution impractical.

In this paper we discuss coupling of MBD and CFD solvers to enable computations of bodies connected with cables, with focus on L&R problems.

2 CFD CODE REX

REX is a general purpose CFD code designed for computational naval hydrodynamics applications, developed at IIHR-Engineering and Hydroscience/The University of Iowa. REX is an unsteady Reynolds-averaged Navier-Stokes, detached eddy simulation (URANS/DES) overset solver that uses a blended model for turbulence, a single-phase level set approach to model the free surface (Carrica et al. 2007a), and dynamic overset grids to resolve large-amplitude motions (Carrica et al. 2007b). The air side is treated with a semi-coupled approach, in which the water ignores the presence of the air but the air is computed using the water free surface as an immerse boundary, providing an excellent approximation to the air flow and forces on large-scale objects like ships (Huang et al. 2008). Overset connectivities are computed at run time using the code Suggar or Suggar++ (Noack et al. 2009), while the surface weights to compute forces and moments are obtained using Usurp (Boger and Dreyer 2006). Full six degrees of freedom (6DOF) rigid-body motion computations with moving control surfaces and resolved or modeled propulsors are possible. The code architecture enables the presence of multiple bodies, which as discussed in this paper allows the simulation of connecting structures such as cables between the different discretized bodies included in the domain. Internal waves, dead water and other density stratification phenomena can be studied with the higher-order density transport model (Esmaeilpour et al 2016, 2017). Other capabilities include incoming regular and irregular waves, autopilot and maneuvering controllers (Carrica et al. 2012), and fluid-structure interaction (Paik et al. 2009; Li et al. 2017). Self-propulsion of surface ships in model scale (Carrica et al. 2010a, Carrica et al. 2011) and at full scale (Castro et al. 2011) have been performed with excellent comparison with data. Surface ship maneuvers in turn and zig-zag with and without waves (Carrica et al. 2013) and in broaching (Carrica et al. 2012) demonstrated the capability of the code to handle complex situations with free surface flows. Recent simulations of KCS maneuvering in deep (Mofidi and Carrica 2014) and shallow water (Carrica et al. 2016a) further validated complex maneuvering capabilities. High-performance computations have been previously performed with grids of up to 300 million grid points for the surface combatant model DTMB 5512 in straight ahead, static drift, forward-speed diffraction and pitching and heaving in waves (Carrica et al. 2010b, Bhushan et al. 2011), and for the crude carrier KVLCC2 on up to 305 million grid points (Xing et al. 2010). New dynamic overset approaches (Martin et al. 2014, Martin et al. 2016) have allowed the calculation of similarly large cases for the fully appended geometry of the research vessel Athena, including a rotating discretized propeller, with excellent scalability of the overset problem. Also new to REX is a complete reformulation of the projection algorithm used for coupling the velocity and pressure fields, resulting in an improved mass conservation compared to the standard projection method (Li et al. 2015). REX have been used for several projects by academic institutions and US Navy researchers.

Boundary layer transition models have been recently implemented and validated. These include those based on intermittency and correlations by Langtry and Menter (2009) and Menter et al. (2015) and the amplification factor approach of Coder and Maughmer (2014). Current implementations have been tested against flat plate geometries, ellipsoids, and propellers. More complex applications and evaluation of best practices and limitations are currently under way.

Fully free running maneuvers have been successfully simulated both using discretized propeller blades and for the REX/PUF-14 coupled approach for underwater vehicles in fully submerged and near calm surface conditions. Satisfactory agreement with available experimental data was obtained for two different geometries, ONR Body1 (Martin et al 2014a,

2015) and Joubert BB2 (Carrica et al 2016b); small differences between simulations and experiments can be attributable to a number of reason including differences in initial conditions, which are beyond the control of the simulation setup; but also to low Reynolds effects, particularly in the control surfaces, which can be investigated with the newly available transitional models.

3 MBD CODE MAGNUSDYN

MagnusDyn is an MBD solver based on a velocity formulation that can handle rigid bodies connected with cables and a variety of constraints, implemented using Lagrange multipliers (see Figure 1). Constraints include ball and hinge joints and imposed rotation joints, this last to facilitate implementation of rotating bodies like propellers or rudders, where the rotation is imposed by the propeller rotational speed or the rudder angle.

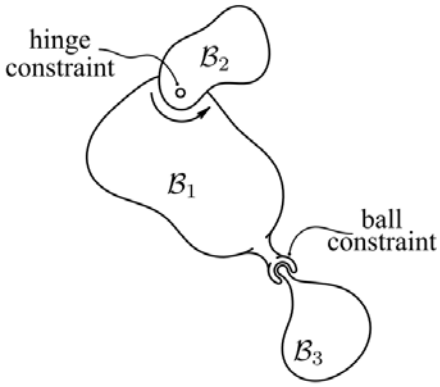

Figure 1: Schematic of a multi-body dynamic system including some constraints.

MagnusDyn uses unit quaternions to parameterize the body rotations; quaternions do not suffer from singularity problems as the Euler angles do. Euler angles use three rotations in sequence to describe any rotation. Several options are available depending on what three rotation sequences are used. In naval and aeronautical engineering the (1,2,3) sequence, also known as Cardan or Tait-Bryan angles, is used. In this sequence first a yaw rotation ψ is applied about the z-axis, then a pitch rotation θ about the y-axis and finally a roll rotation φ about the x-axis. Since REX uses Euler angles for several applications, as customary in naval architecture, angular representation is transformed when going from REX to MagnusDyn and back. A cable solver is constructed within MagnusDyn using cylindrical links connected with ball constraints. The cable solver accepts external forces and moments on each link as computed by the CFD solver. It also can move an end node on a cable to a specified location, to simulate reel-in and release.

3.1 CFD/MBD coupling

The coupling between CFD and MBD requires computation of forces and moments in the CFD code and transfer to the MBD code, and prediction of motions in the MBD code and transfer back to the CFD code. The MBD code receives the forces and moments respect to the center of gravity for each body, computed by integration in the CFD code, and advances as many time steps as necessary to complete a CFD time step. During this period the forces and moments are considered constant, except for the cable forces and moments as described later.

At the end of a CFD time step the MBD code sends the information on body translation and rotation, including the location of all cable links, to the CFD code. The CFD code uses this information to move the grids belonging to each body, and to retrieve the velocity corresponding to each cable link.

An inverse map is used to efficiently find fluid velocities to use to compute fluid forces on the links of the cables. REX uses a simple uniform Cartesian grid within the bounding box of each domain after the grid is decomposed into in-processor domains for parallel processing. The proper donor points laying within each cell of the Cartesian grid are found. If no point is found, neighbors are used to fill the remaining otherwise empty cells, in a closest-neighbor-first fashion. The setup of the inverse map is then done only once at the beginning of the computation and is done independently for each decomposed grid. For each i,j,k node in the Cartesian grid, the inverse map contains the i,j,k of the closest CFD grid point in the grid belonging to that processor. Since x,y,z for each i,j,k cell in the Cartesian grid can be explicitly obtained and vice versa, finding i,j,k in the Cartesian grid given the coordinates of a point is extremely fast.

Once the location of the links is obtained by the cable simulation processor, these locations are transformed to the original system of coordinates before body motions and broadcasted to all other processors. The inverse map is used to find the donor in each CFD grid. Processors will report that a donor was found in the grid belonging to that processor if the point is within the original bounding box. Since in an overset approach several grids can have valid donors, the best donor is chosen prioritizing points that are active (as opposed to fringe; blanked points are not valid donors) and those closest to the original link location. The velocities are then sent to the MBD solver which computes the forces and moments on the links implicitly, since these forces and moments depend on the velocity and acceleration of the links.

4 RESULTS

4.1 Rising buoy in a tank

This simulation reproduces the experimental conditions reported in the work by Kamman and Huston (1985). In this experiment a buoy with mass $m_b = 11.31gr\ (0.025lb)$ and 2 inches in diameter $D_b = 50.8mm$ is attached to the bottom of a tank with a silicon rubber cable 72 inches ($l_c = 1.829m$) in length and diameter $D_c = 4.14mm$. The tank is filled with seawater with density and viscosity are $\rho_w = 1024\,Kg/m^3$ and $\mu_w = 1.684\times10^{-3}\,Kg/m.s$, respectively.

The grids and initial condition are shown in Figure 2. The initial position of the buoy is $x_b^0 = (51in, 0, -24in)$ as reported by Kamman and Huston (1985), but the position of the fixed point $x_f = (0, 0, -75.6in)$ is inferred from their experimental results since it is not explicitly reported. The entire setup is under water far from the surface.

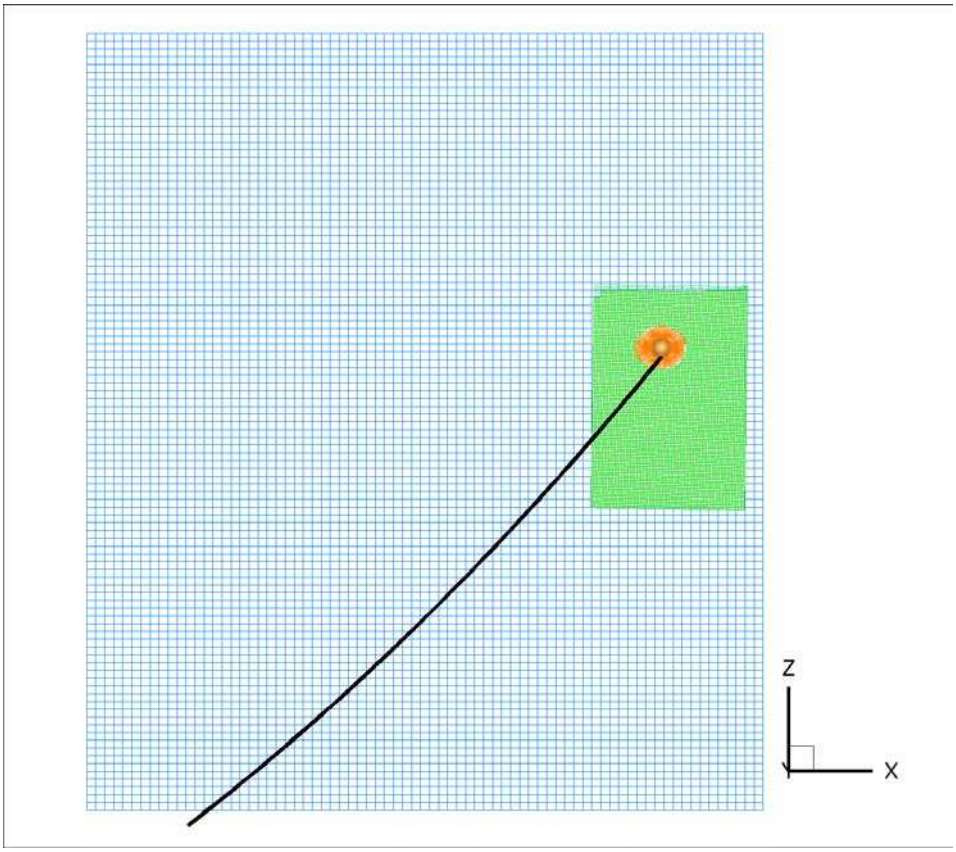

Figure 2: Grids and initial condition for the rising buoy case.

As exact experimental data is not available, the cable initial configuration is set to be that of a catenary between the fixed point at the bottom of the tank and the bottom of the buoy. While this is a good assumption (see Figure 3), small deviations from the catenary are likely in the experiment at the ends of the cable. Notice that in this initial configuration the buoy early tendency will be to rotate in the clockwise direction (positive pitch) due to the tension of the cable. Probably a better initial condition would be that of a buoy with pitch angle so that the cable is at rest even if the buoy is free to rotate (but not to move). In this example the importance of this initial rotation is evaluated by running the same case twice; one with the buoy free to rotate and one where rotations are constrained.

The diameter of the buoy is used as the reference length, $L_0 = D_b = 50.8mm$. The reference velocity is arbitrarily set to $U_0 = 1m/s$. With the stated density and viscosity of seawater the Reynolds and Froude number result in $\mathrm{Re} = 30,890$ and $Fr = 1.416$, respectively. The dimensionless mass of the buoy is $m_b^* = m_b / \rho_w L_0^3$. Since the buoy essentially is a thin shell, all the gyradii equal to the buoy's radius, which in dimensionless form is $R_b^* = 0.5$.

The mass of the cable, or its linear density, are not properly reported by Kamman and Huston (1985) and therefore this is inferred from the reported forces when the buoy reaches a steady condition at the top. In that situation the force measured at the fixed point is the buoyancy force on the buoy plus the buoyancy force on the cable minus the weight of the buoy and the cable. Since buoy weight and buoyancy are known, the density of the cable is estimated to be $\rho_c = 1280\,Kg/m^3$, which is in close agreement with reported values of density for silicon rubber. The linear density is then $\lambda_c = \rho_c \pi / 4 D_c = 17.23 gr/m$.

The simulations are performed with 60 links for the cable. Figure 3 shows the computed positions of the cable at different times compared with experiments reported in Kamman and Huston (1985) (Figure 4). Both computational results, with and without buoy's rotations are shown. The small differences between the two solutions in Figure 3 indicate that the effects of buoy's rotations in the overall solution are small, while the computational results march the experiments very well.

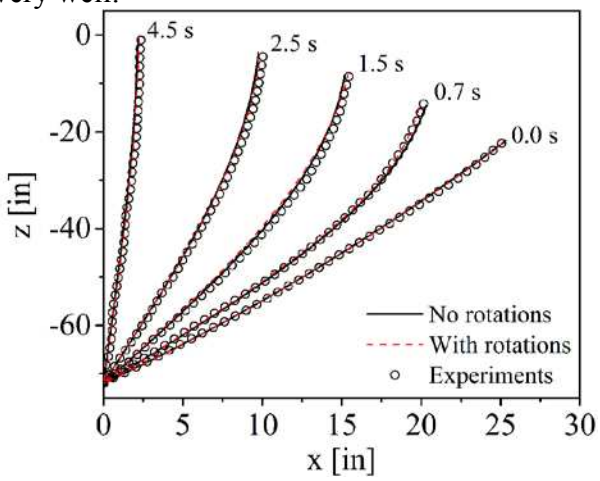

Figure 3: Cable position with time. Comparison of results with and without buoy rotations with experiments.

Figure 4 compares the tension in the cable computed at the fixed end located at the bottom of the tank with the tension measured in the experiment (from Figure 10 in Kamman and Huston, 1985). Forces undergo a more violent transient when buoy rotations are allowed, as expected. The amplitude of the oscillations in the initial transient seem to be in agreement with the variations observed in the initial transient of the experimental data. As expected, both computations with and without buoy rotation converge to the same steady state tension in the cable when the buoy is all the way at the top of the tank.

Figure 5 shows a series of still frames at the corresponding times reported in the experiments as in Figure 3. During the initial transient the boundary layer around the sphere develops and eventually starts separating resulting in vortex shedding. This vortex shedding affects the motion of the sphere, resulting in oscillations in forces.

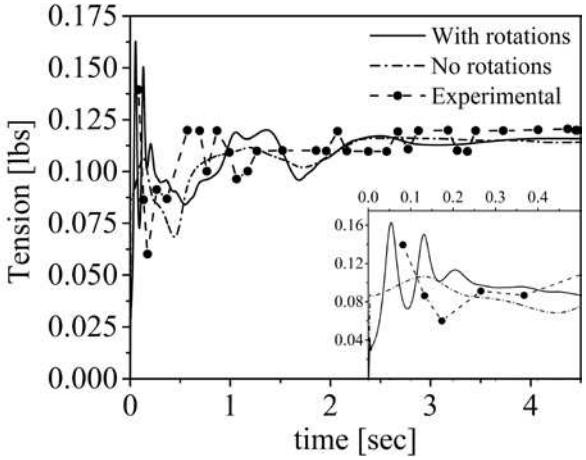

Figure 4: Cable tension at the fixed end compared with experimental measurements. Both results with and without buoy rotations are shown.

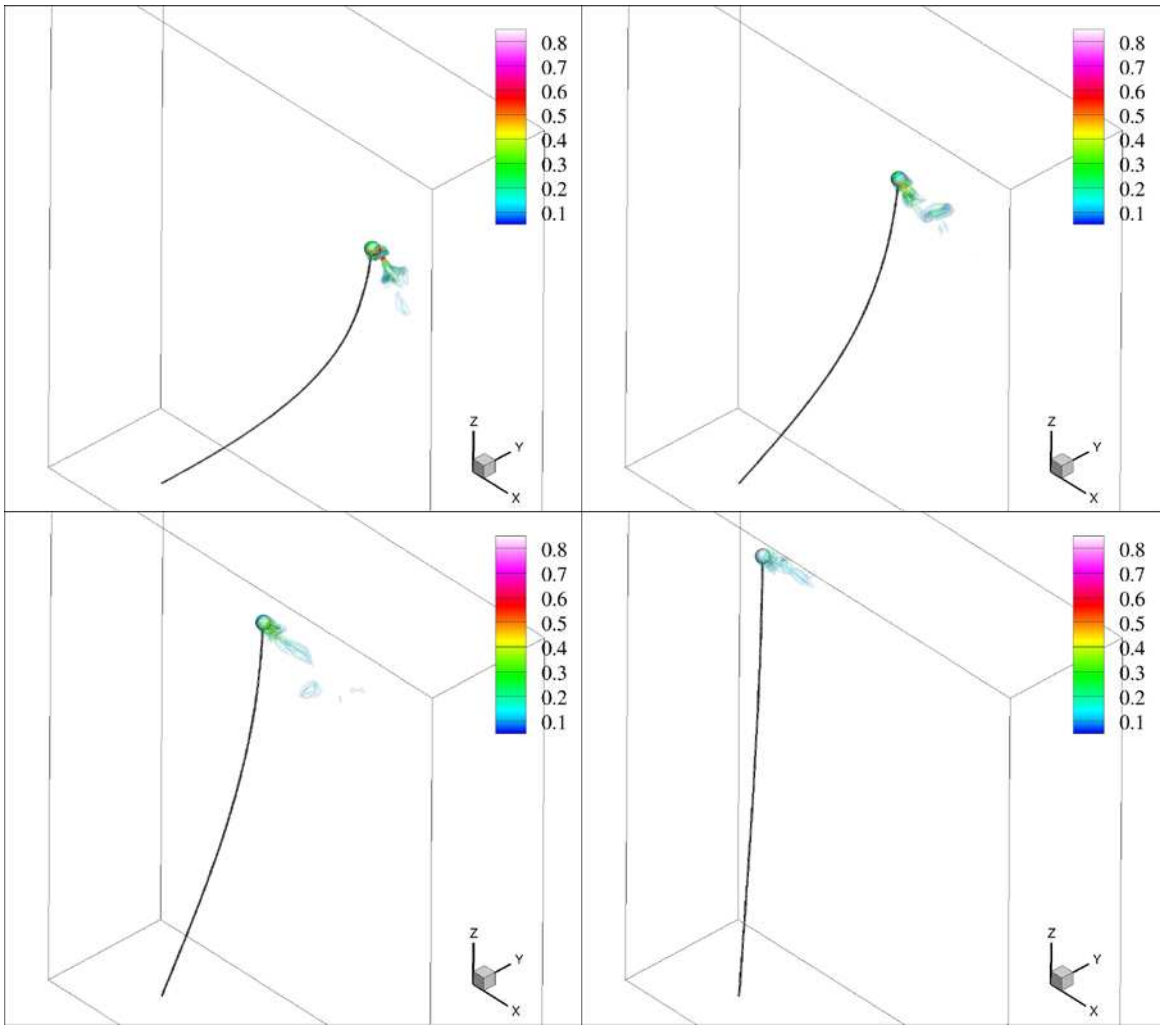

Figure 5: Still frames corresponding 0.7, 1.5, 2.5 and 4.5 s (from top to bottom, left to right).

4.2 Deployment of an UUV

In this case the research vessel Athena (Athena R/V) is used as mother ship to deploy an UUV from a crane, lowering it slowly until it reaches the water and then releasing it. For non-dimensionalization purposes the reference velocity and length are $U_0 = 5.4 m/s$ (10.5 knots) and $L_0 = 47m$, respectively.

Figure 6 (left) shows the geometry of the system. Athena R/V is fully appended and includes movable rudders and rotating discretized propellers. The UUV grids were originally created with the UUV nose pointing to the port side of Athena. This is changed as part of the initial conditions so that the UUV points forward and is farther away from the stern of Athena to avoid a collision, as occurs in preliminary computations if the UUV is released to close to the stern in the region of strong recirculating flow. The UUV is followed by a Cartesian refinement block (shown in orange in Figure 6). A free surface refinement (shown in blue) follows the motions of the mother ship in the horizontal plane only. A wake refinement (shown in Cyan) follows the ship motions to properly resolve the wakes of the propellers. A detail of the UUV grids with refinements is shown in Figure 6 (right), where the UUV is already positioned and rotated with its nose pointing into Athena's stern. The total number of grid points for this case is 32M. Figure 6 also shows the crane system and cables holding the

UUV in the initial condition.

Cables are laid out by first defining nodes in space. Once nodes are defined cables are described with a starting and an ending node. With this information and the provided length of the cable the MBD solver creates a catenary between the starting and ending points with the specified length.

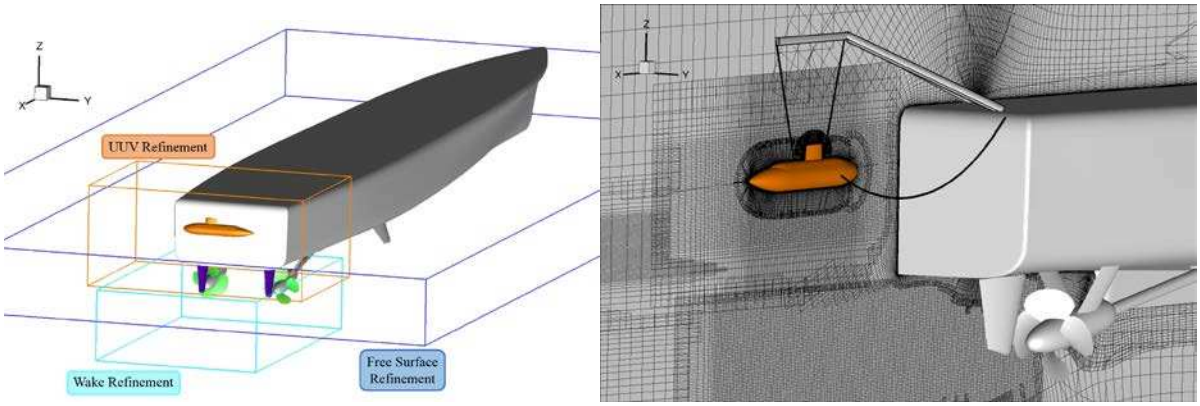

Figure 6: Geometry and refinement blocks used for the deployment of an UUV from the stern of Athena R/V (left); Close up of the system of grids for the UUV. The UUV was repositioned and rotated as an initial condition to start the simulation (right).

The cables are modeled as wire rope ¾ inches in diameter with linear density $\lambda_c = 1.5 Kg/m$ of 1.5 Kgr/m. The number of cable links is set to 45, so that the curvatures are properly resolved.

Simulation conditions are set for incoming head irregular waves modeled with a Bretschneider spectrum, mimicking a sea state 3 situation. An autopilot including PI speed and heading controllers is used, acting on the angle of the rudders and rotational speed of the propellers, respectively. Targets for the autopilot are a speed of 4.5 knots and 0 degree (north) heading.

The dimensionless time step is set to $\Delta t = 0.00015$. The simulation is started with the UUV hanging and free to move, while the speed controller actuates to accelerate the ship. The cable is then slowly deployed until the UUV is stable in the water, at which point the UUV is released. It is stressed that the MBD solver treats all bodies (ship, propellers and rudders, UUV, cable links, etc.) as interacting, thus the forces and moments caused by hanging the UUV are fed to the mother ship.

Figure 7 shows a sequence of images as the UUV is lowered and released. Vortical structures are shown as isosurfaces of the second invariant of the velocity gradient tensor, $Q = 5000$ colored with longitudinal (U) velocity. As the rotational speed of the propellers changes to maintain the target speed of 10.5 kn with varying wave resistance, the thrust and generation of propeller tip vortices fluctuates. Ship roll and UUV swinging can be observed in the time-evolving panels.

Figure 8 shows time histories of heading, roll, pitch and rudder angles for the mother ship Athena R/V. Rudder excursions of approximately 5 degrees are necessary to maintain course within 1 degree of target. The ship rolls with amplitude of approximately 5 degrees and period of 0.5 s (dimensionless, 4.35 s dimensional), exhibiting a pitching amplitude of about 1 degree. These motions have a considerable effect on the motions and forces affecting the UUV, shown in Figure 9. The UUV experiences roll and pitch angles larger than the mother

ship, as it swings while hanging. Once it touches the water, one of the cables suffers a considerable jerk at 1.95 s, observable in Figures 7 and 9. At approximately 2.25 s the UUV is released.

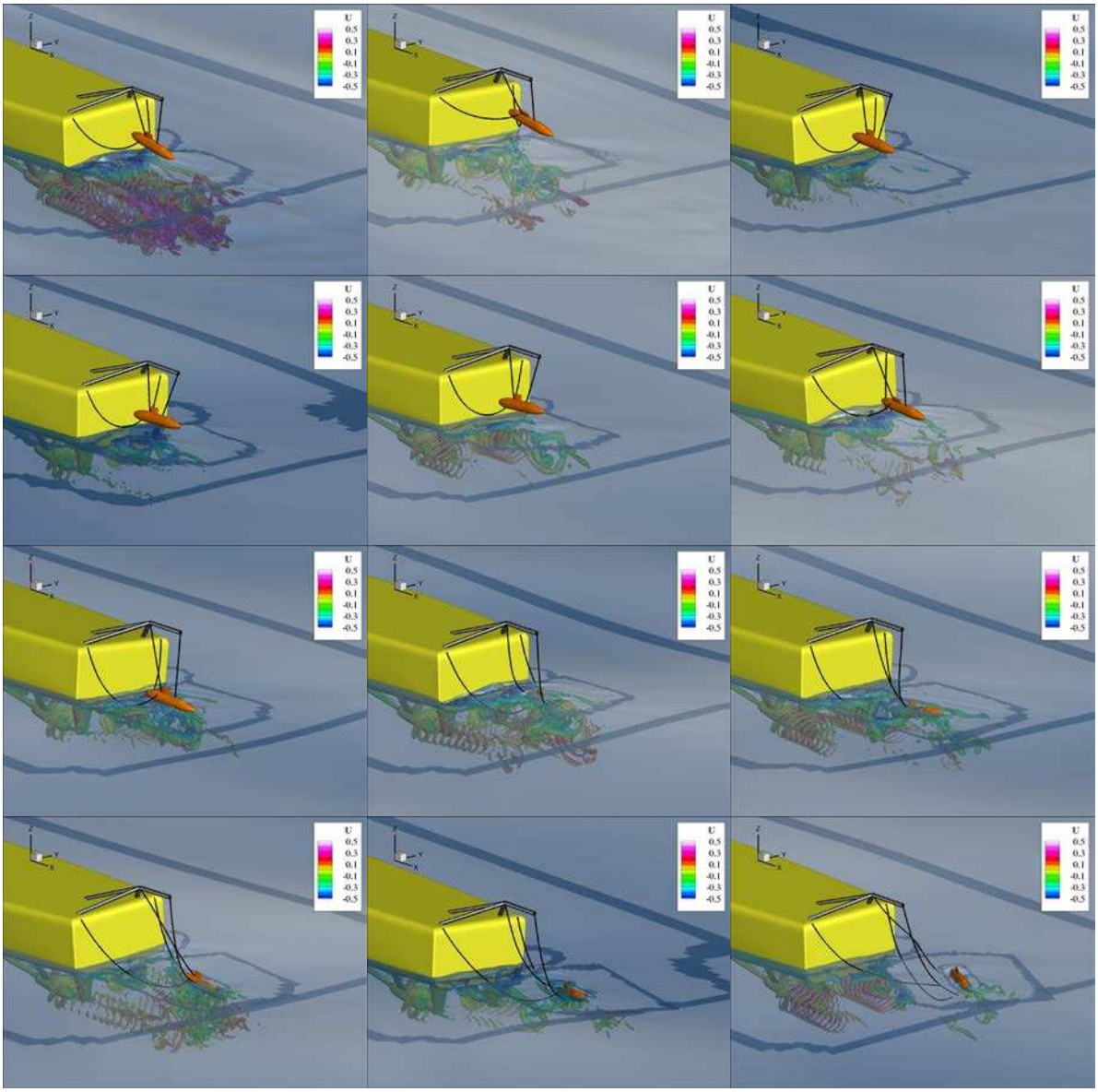

Figure 7: UUV deployment is sea state 3. From top to bottom, left to right, frames at 0.6, 0.75, 0.9, 1.05, 1.2, 1.35, 1.5, 1.65, 1.8, 1.95, 2.1 and 2.25 dimensionless seconds.

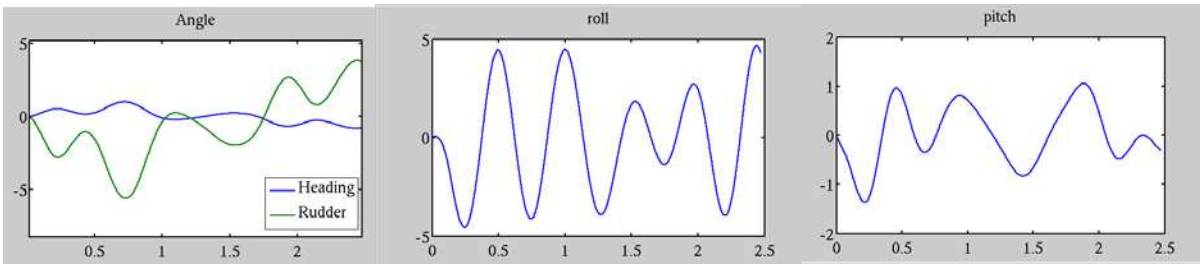

Figure 8: Time histories of motions of Athena R/V: heading and rudder angles (left), roll (center) and pitch (right).

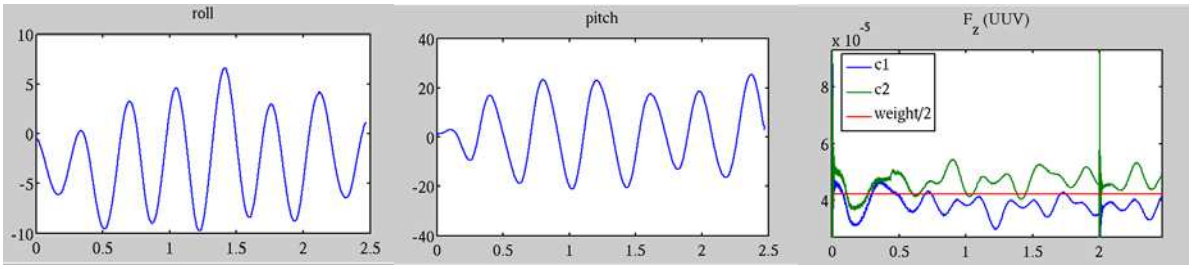

Figure 9: Time histories of motions of the UUV: roll (left), pitch (center) and cable dimensionless forces (right).

4.3 Recovery of an AUV

The problem under study is the recovery of an autonomous underwater vehicle (AUV) from the stern of a mother ship. The AUV is captured from a crane with an electromagnetic lift attached to a piece of wire rope. As in the case of UUV deployment in section 4.2, the mother ship is represented by Athena R/V. In this case Athena R/V is set with a cruise controller to attain a target speed of 5 knots and 0 degree heading in a sea state 4 condition. The total number of grid points for CFD is approximately 40M.

The AUV has an autopilot with a head-to-point controller that attempts to follow a meeting point 1 m behind the stern of Athena R/V and on the centerplane. The 3-bladed propeller rotational speed is regulated by a PI controller to approach the meeting point, while the heading is set with a PID controller acting on the rudders so that the AUV points toward the meeting point. The demands on the autopilot controllers are high, with the mother ship moving in all degrees of freedom. In addition the stern region of the mother ship is highly turbulent at low speeds, exhibiting a recirculating zone that attracts the AUV toward the ship if it gets close. The crane system automatically engages the electromagnetic lift if the AUV is within a certain short distance from the meeting point and the AUV is moving at a relative velocity less than a given operational limit.

Figure 10 shows a time sequence of the process of recovery, with vortical structures shown as isosurfaces of $Q = 5000$ colored with U velocity. The AUV makes several failed attempts at reaching the meeting point before it is positioned within capturing distance. When that occurs the electromagnetic lift attaches to the AUV, connecting the AUV with the cable connected to the crane, and through it to the mother ship.

5 CONCLUSIONS

Coupling of a CFD code with an MBD solver was described. Three examples were presented: a rising buoy, used also for validation of the implementation, and deployment of an UUV and recovery of an AUV. Comparison with data for the buoy rising problem was satisfactory, while the ability to simulate complex cable/body problems demonstrated a unique capability.

While the number of tasks involved in implementing CFD/MBD coupling is considerable, the main challenge was to maintain stability in view of the different demands in time of both solvers when cables are exposed to jerks. This was achieved by fully coupling all bodies in the MBD system, and by improving integration in the MBD solver and enabling time steps consistent with the transients to be resolved.

Future work involves addition of contact detecting algorithms and contact models to the multibody dynamics solver, to add capability to simulate a wide variety of problems, like

landing of aircraft in moving ships, beaching of amphibious vehicles, push-tow ship configurations, etc. In addition, direct gridding of the cables can enable simulation of flow-induced vibrations, of interest for a variety of applications, while fluid forces on the cables will be directly predicted instead of being modeled.

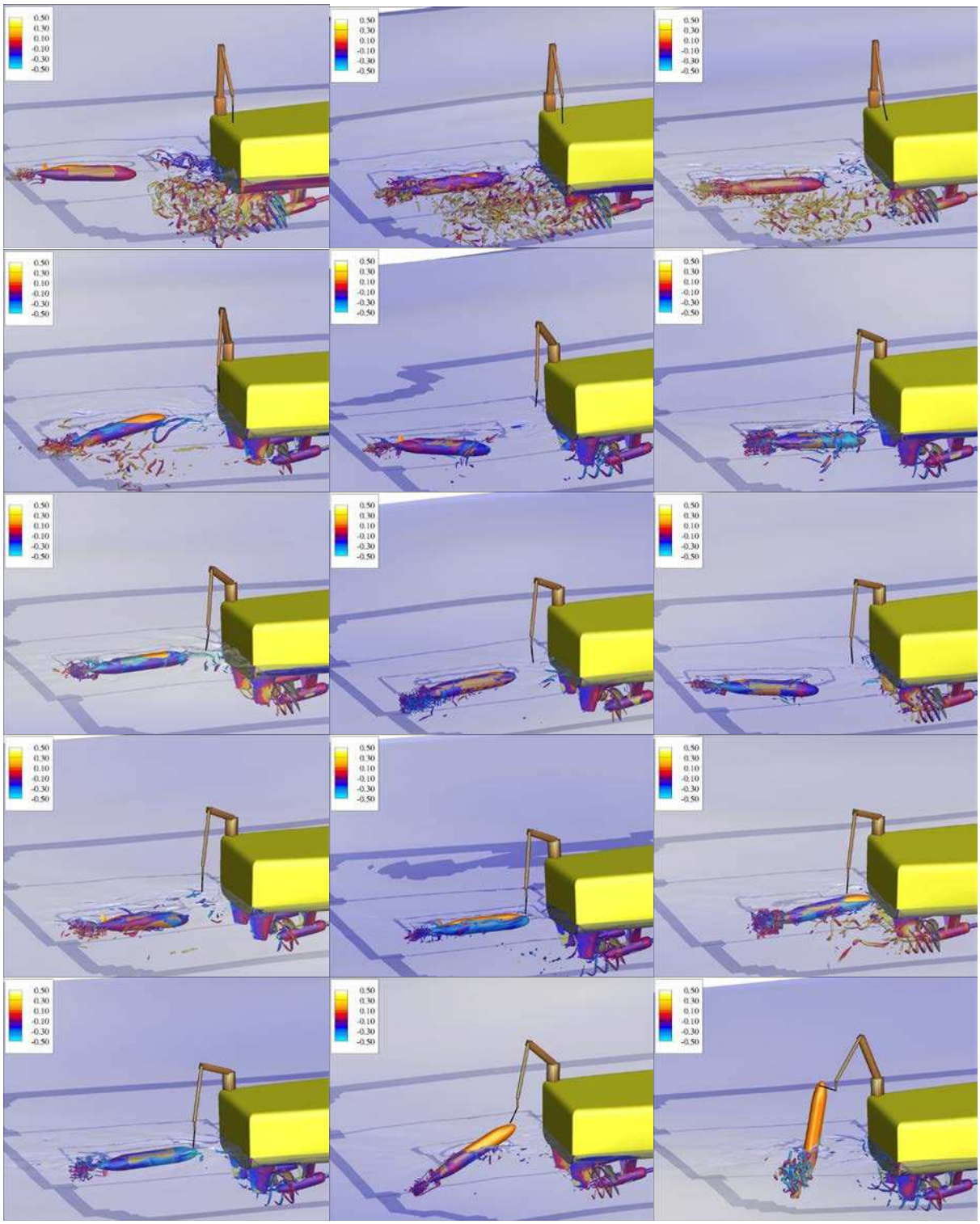

Figure 10: AUV recovery is sea state 4. From top to bottom, left to right, frames at 0.3, 0.6, 0.9, 1.2, 1.5, 1.8, 2.1, 2.4, 2.7, 3.0, 3.3, 3.6, 3.9, 4.2 and 4.5 dimensionless seconds.

REFERENCES

Boger, D.A., and Dreyer, J.J., Prediction of Hydrodynamic Forces and Moments for Underwater Vehicles Using Overset Grids. AIAA paper 2006-1148, *44th Aerospace Science Meeting*, Reno, NV, 2006.

Bhushan, S., Carrica, P.M., Yang, J., and Stern, F., Scalability and Validation Study for Large Scale Surface Combatant Computations Using CFDShip-Iowa. *International Journal of High Performance Computing and Applications*, 25:466-487, 2011.

Carrica, P.M., Wilson, R., and Stern, F., An unsteady single-phase level set method for viscous free surface flows. *International Journal for Numerical Methods in Fluids* 53:229-256, 2007a.

Carrica, P.M., Wilson, R.V., Noack, R., and Stern, F., Ship motions using single-phase level set with dynamic overset grids. *Computers and Fluids*, 36:1415-1433, 2007b.

Carrica, P.M., Castro, A.M., and Stern, F., Self-Propulsion Computations Using Speed Controller and Discretized Propeller with Dynamic Overset Grids. *Journal of Marine Science and Technology*, 15:316-330, 2010a.

Carrica, P.M., Huang, J., Noack, R., Kaushik, D., Smith, B., and Stern, F., Large-Scale DES Computations of the Forward Speed Diffraction and Pitch and Heave Problems for a Surface Combatant. *Computers and Fluids* 39:1095-1111, 2010b.

Carrica, P.M., Fu, H., and Stern, F., Computations of self-propulsion free to sink and trim and of motions in head waves of the KCS Container Ship model. *Applied Ocean Research*, 33:309-320, 2011.

Carrica, P.M., Sadat-Hosseini, H., and Stern, F., CFD Analysis of Broaching for a Model Surface Combatant with Explicit Simulation of Moving Rudders and Rotating Propellers. *Computers and Fluids* 53:117-132, 2012.

Carrica, P.M., Ismail, F., Hyman, M., Bhushan, S., and Stern, F., Turn and Zigzag Maneuvers of a Surface Combatant Using a URANS Approach with Dynamic Overset Grids. *Journal of Marine Science and Technology*, 18:166-181, 2013.

Carrica, P.M., Mofidi, A., Eloot, K., and Delefortrie, G., Direct Simulation and Experimental Study of Zigzag Maneuver of KCS in Shallow Water. *Ocean Engineering* 112:117-133, 2016a.

Carrica, P.M., Kerkvliet, M., Quadvlieg, F., Pontarelli, M., and Martin, J.E., CFD Simulations and Experiments of a Maneuvering Generic Submarine and Prognosis for Simulation of Near Surface Operation. *31st Symposium on Naval Hydrodynamics*, Monterey, CA, 2016b.

Castro, A.M., Carrica, P.M., and Stern, F., Full scale self-propulsion computations using discretized propeller for the KRISO container ship KCS. *Computers and Fluids* 51:35-47, 2011.

Coder, J.G., and Maughmer, M.D., Computational Fluid Dynamics Compatible Transition Modeling Using an Amplification Factor Transport Equation. *AIAA Journal*, 52:2506-2512, 2014.

Esmaeilpour, M., Martin, J.E., and Carrica, P.M., Near-Field Flow of Submarines and Ships Advancing in a Stable Stratified Fluid. *Ocean Engineering*, 123:75-95, 2016.

Esmaeilpour, M., Martin, J.E., and Carrica, P.M., Computational Fluid Dynamics Study of the Dead Water Problem. *Journal of Fluids Engineering*, accepted, 2017.

Huang, J., Carrica, P.M., and Stern, F., Semi-coupled air/water immersed boundary approach for curvilinear dynamic overset grids with application to ship hydrodynamics. *International*

Journal for Numerical Methods in Fluids, 58:591-624, 2008.

Kamman, J.W., and Huston, R.L., Modelling of submerged cable dynamics. *Computers and Structures*, 20(1-3):623-629, 1985.

Langtry, R.B., and Menter, F.R., Correlation-Based Transition Model for Unstructured Parallelized Computational Fluid Dynamics Codes. *AIAA Journal*, 47:2894-2906, 2009.

Li, J., Castro, A.M., and Carrica, P.M., "A pressure-velocity coupling approach for high-void fraction free surface bubbly flows. *International Journal for Numerical Methods in Fluids*, 79:343-369, 2015a.

Li, Y., Castro, A.M., Martin, J.E., Sinokrot, T., Prescott, W., and Carrica, P.M., Coupled Computational Fluid Dynamics/Multibody Dynamics Method for Wind Turbine Aero-Servo-Elastic Simulation including Drivetrain Dynamics. *Renewable Energy*, 101:1037–1051, 2017.

Martin, J.E., Noack, R., and Carrica, P.M., Multiple Body Overset Connectivity Method with Application to Wind Farm Simulations. *12th Symposium on Overset Composite Grids and Solution Technology*, Atlanta, GA, 2014a.

Martin, J.E., Michael, T., and Carrica, P.M., Overset Simulations of a Submarine in Self-Propelled and Maneuvering Conditions. *30th Symposium on Naval Hydrodynamics*, Hobart, Australia, 2014b.

Martin, J.E., Michael, T., and Carrica, P.M., Submarine Maneuvers Using Direct Overset Simulation of Appendages and Propeller and Coupled CFD/Potential Flow Propeller Solver. *Journal of Ship Research* 59(1):31-48, 2015.

Martin, J.E., Esmaeilpour, M., and Carrica, P.M., Near-Field Wake of Surface Ships and Submarines Operating in a Stratified Fluid. *31st Symposium on Naval Hydrodynamics*, Monterey, CA, 2016.

Menter, F.R., Smirnov, P.E., Liu, T., and Avancha, R., A One-Equation Local Correlation-Based Transition Model. *Flow, Turbulence and Combustion*, 95(4):583-619, 2015.

Mofidi, A., and Carrica, P.M., Simulations of Zigzag Maneuvers for a Container Ship with Direct Moving Rudder and Propeller. *Computers and Fluids* 96:191-203, 2014.

Noack, R., Boger, D., Kunz, R., and Carrica, P.M., Suggar++: An Improved General Overset Grid Assembly Capability," AIAA Paper 2009-3992, *19th AIAA CFD Conference*, San Antonio, TX, 2009.

Paik, K., Carrica, P.M., Lee, D., and Maki, K., Strongly coupled fluid–structure interaction method for structural loads on surface ships. *Ocean Engineering*, 36:1346-1357, 2009.

Xing, T., Carrica, P.M., and Stern, F., Large-Scale RANS and DDES Computations of KVLCC2 at Drift Angle 0 Degree. *CFD Workshop Gothenburg 2010*, Gothenburg, Sweden, 2010.